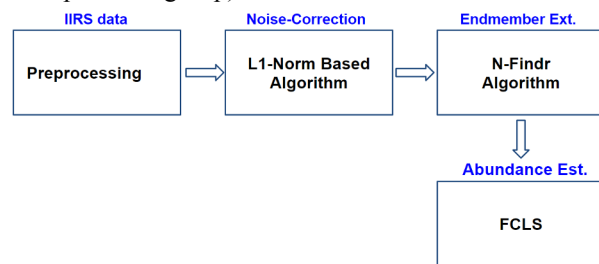


**Spectral Unmixing and Abundance estimation of different Pyroxene Species using IIRS Chandrayaan-2 Hyperspectral Imagery.** Touseef Ahmad\*, Tathagata Chakraborty, Rosly B Lyngdoh, Satadru Bhattacharya, Patil Abhishek N, Ankush Kumar, Arup Benarjee, Praveen K Gupta, and Arundhati Misra, Space Applications Centre, Indian Space Research Organization, Ahmedabad, India \*(touseef@sac.isro.gov.in)

**Introduction:** The pyroxene mineralogy on the lunar surface can be characterized by low and high calcium variety. Differentiating and mapping the distribution of these pyroxene species is crucial for understanding lunar crustal evolution. Hyperspectral imagery (HSI) played a significant role in deciphering the distribution of lunar minerals characterizing their spectral features [e.g. 1-6]. ISRO's Imaging Infrared Spectrometer (IIRS) sensor onboard Chandrayaan-2 orbiter is an advanced hyperspectral imaging spectrometer with capability to collect spectra for a longer spectral range (800 nm to 5000 nm) at very high spatial resolution (~80m) and spectral resolution (~20-25nm) [7]. In the present study, we tried to denoise the IIRS infrared spectra and further utilize the denoised spectra to unmix the contributions of low and high calcium pyroxene at spectral level. Finally, we estimate the abundance of these pyroxene species at subpixel level to generate the abundance map corresponding to various pyroxene species and regoliths.

**Study Area and Data used:** The region is situated in the East and South-East of Taurus-Littrow valley and the southeastern end of the analyzed image covers western flank of Gardner crater. Level 1 radiometrically calibrated IIRS radiance subset with line-1105, sample-250 and channel-101, is utilized to analyze lunar mineralogy. The infrared spectra (800nm - 2500nm), after initial radiometric calibration is converted to reflectance spectra by normalizing with solar flux (Fig. 1: Preprocessing step).



**Figure 1:** Flow-chart for spectral unmixing analysis using IIRS data.

**Methodology:** The IIRS reflectance spectra are denoised and further utilized for unmixing and mineral abundance map generation based on the following techniques (Fig. 1).

**i. Spectral Denoising:** Actually, IIRS Ch-2 HSIs have been corrupted by additive mixed noise, i.e.,

mixture of Gaussian noise, impulse noise, and stripes in the acquisition process. An  $L_1$ -norm based denoising algorithm [8] was used which is the latest state-of-the-art algorithm for removing mixed noise from HSI. This algorithm deals with mixed noise having a complex statistical distribution using robust  $L_1$  data fidelity terms instead of  $L_2$  data fidelity, which is commonly employed for Gaussian noise removal. This algorithm also fully exploits a compact and sparse HSI representation based on its low-rank and self-similarity characteristics.

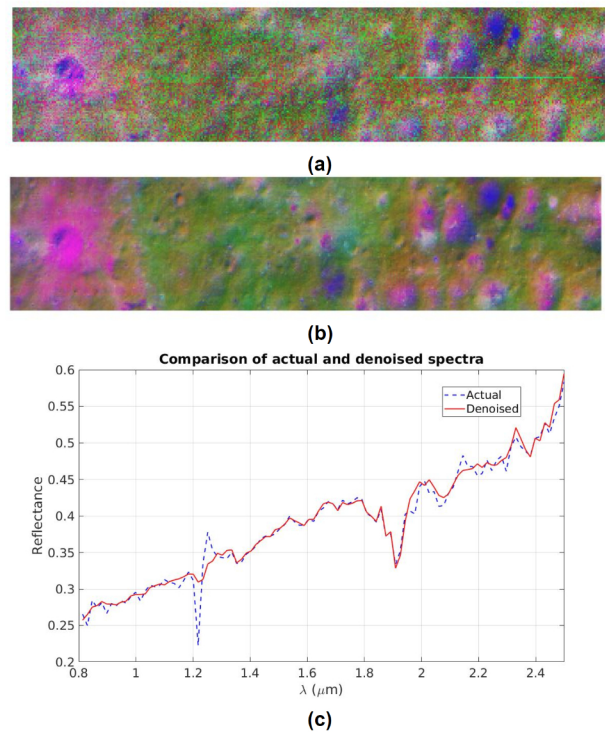


**Figure 2:** (a) False Colour Composite (1700nm, 2210nm, 2310nm) of original IIRS data, (b) False Colour Composite (1700nm, 2210nm, 2310nm) of denoised IIRS data, (c) Comparison of original and denoised spectra of random pixel.

**ii. End-member Extraction:** The analysis of hyperspectral data sets necessitates the identification of specific basis spectra known as endmembers. Once these spectra have been identified, the HSI can be decomposed into the fractional abundance of each material in each pixel. There are several techniques for determining the end-members, the majority of which require the intervention of a trained geologist. These end-members are assumed to be present in the image as pure or unmixed pixels. The N-Findr [9], a convex

geometry-based endmember extraction algorithm, is employed in this paper to determine a unique set of purest pixels in HSI. This technique is based on the fact that the N-volume contained by a simplex formed of the purest pixels in N-spectral dimensions, is larger than any other volume formed from any other combination of pixels. The algorithm works by inflating a simplex inside the data, beginning with a random set of pixels.

**iii. Abundance Estimation:** The Linear mixing model (LMM) is widely used for fractional abundance estimation of materials in hyperspectral unmixing analysis. It generally requires two constraints imposed on the LMM, which are the abundance sum-to-one constraint and the abundance non-negativity constraint. The first constraint requires the sum of the abundance fractions of materials present in an image pixel to be one and the second imposes a constraint that these abundance fractions be nonnegative. While the first constraint is easy to deal with, the second constraint is difficult to implement since it results in a set of inequalities and can only be solved by numerical methods. In this context, a fully constrained least square (FCLS) method [10] was used for fractional abundance estimation corresponding to each endmembers.

**Results & Discussion:** In the present study, we minimize the sparse noise content in the original IIRS image and further determine the pure pixel mineral end members (EM) and respective pixel level fractional abundance map using unmixing method. Figure 2 reveals the effectiveness of the denoising technique to generate an analysis ready denoised IIRS image (Figure 2b). The noisy spectrums are smoothened retaining the absorption features (Figure 2c).

The IIRS image majorly consists of smooth regolith with few impact craters. Our analysis deciphered four end members within the image (Figure 3a):

EM-1: Low-Calcium Pyroxene (~Pigeonite in Figure 3b), consist of sharp absorption features with band centers at 950 nm and 2000 nm.

EM-2: High-Calcium Pyroxene (~Augite in Figure 3b), contains broad absorption features with band centers at 1000 nm and 2300 nm.

EM-3: Regolith within crater-wall (younger soil), retaining faint absorption features of pyroxene.

EM-4: Matured Regolith (old soil), almost flat spectra with no prominent absorption features.

Figure 3c depicts the fractional abundance map Ab1, Ab2, Ab3 and Ab4 corresponding to end-member 1, 2, 3 and 4 respectively. EM-1 and EM-2 are majorly limited within impact craters, where, EM-1 i.e. low calcium pyroxene is restricted within a small crater (Ab1). The high calcium pyroxene (i.e. EM-2) is located on the wall of the relatively large crater (Ab2). The unmixing

technique is extremely effective to nullify the spectral features from unwanted origin. Hence, the distribution of the end members in the abundance maps are much more prominent and precise. Mixed mineralogy is observed in lunar crust caused due to mixing of original crust with the excavated material from impacts, impactor mineral and impact melt mineral species. Detailed analysis of crater mineralogy will provide better understanding towards distribution of low calcium pyroxene (high temperature) and high calcium pyroxene (intermediate temperature).

The analysed image is the floor of a heavily degraded crater, where the crater wall retains immature regolith (i.e. Ab3), whereas the crater floor holds the matured featureless regolith (i.e. Ab4). Soil cannot stay for a longer duration on the crater wall to experience complete degradation. Due to gravitational pull and lunar shakes, the soil creeps along the crater wall and finally deposits in the floor section. Hence, the crater wall consists of younger regolith, whereas the crater floor holds the matured regolith.

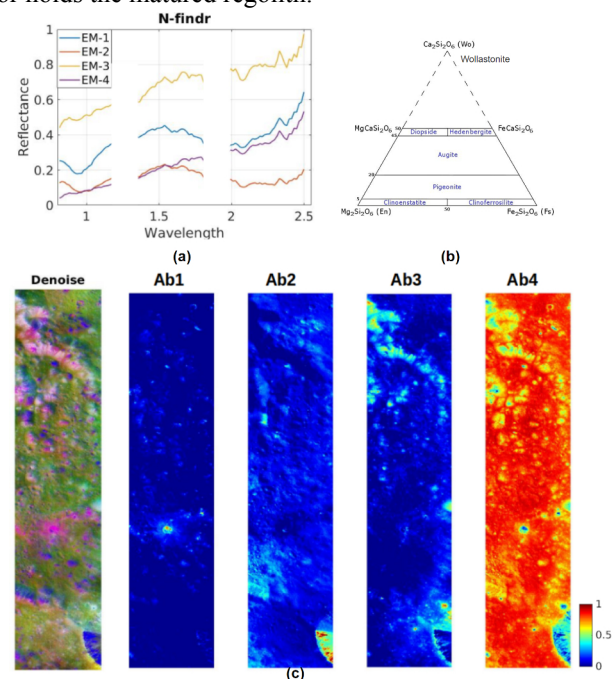


**Figure 3:**(a) Extracted endmembers using N-Findr, (b) Mg-Fe-Ca Pyroxene classification diagram, (c) FCC of denoise image and estimated abundance maps using FCLS.

**References:** [1] Burns R. G. (1993) Cambridge University Press, New York. 551p. [2] Lal D. et al. (2011) LPS XXXXII, Abstract #1339. [3] P. Chauhan et al. (2021) Curr. Sci. 121 (3), 391-401. [4] Ohtake et al. (2009) Nature, 461, 236-240. [5] Pieters C. M. et al. (2009) Science, 326, 568-572. [6] Bhattacharya et al. LPSC 52nd(2021), Abstract#1848. [7] Arup R. C. et al (2020) Curr. Sci. 118, 3, 368-375. [8] Zhuang et al. (2020) IEEE J-STARS, 13, 1143-1157. [9] Winter (1999), Proc. SPIE Imaging Spectrometry, 3753, 266-75. [10] Heinz et al.(2001), IEEE TGRS, 39 (3), 529-545.